Appl. Phys. B 78, 711–717 (2004)
DOI: 10.1007/s00340-004-1467-9

Applied Physics B
Lasers and Optics

I. DOTSENKO✉
W. ALT
S. KUHR
D. SCHRADER
M. MÜLLER
Y. MIROSHNYCHENKO
V. GOMER
A. RAUSCHENBEUTEL
D. MESCHEDE

Application of electro-optically generated light fields for Raman spectroscopy of trapped cesium atoms

Institut für Angewandte Physik, Universität Bonn, Wegelerstr. 8, 53115 Bonn, Germany

Received: 19 September 2003/
Revised version: 27 January 2004
Published online: 26 March 2004 •

ABSTRACT We present an apparatus for generating a multi-frequency laser field to coherently couple the $F = 3$ and $F = 4$ ground state of trapped cesium atoms through Raman transitions. We use a single frequency diode laser and generate sidebands by means of a 9.2 GHz electro-optic modulator. With an interferometer, we separated the sidebands and carrier, sending them to the trapped atoms in opposite directions. The Rabi oscillation of the populations of $F = 3$ and $F = 4$ is monitored. We find that due to destructive quantum interference of two simultaneous Raman transitions the expected Rabi frequency is reduced by a factor that is in quantitative agreement with theoretical expectations. It is demonstrated how this interference can be suppressed experimentally. Besides, we demonstrate the application of the setup for Raman spectroscopy of Zeeman sublevels and of the vibrational states of a small number of trapped atoms.

PACS 32.80.Pj; 32.80.Qk; 42.50.Ct

1 Introduction

Stimulated Raman transitions coupling ground state hyperfine levels are a versatile tool to manipulate laser-trapped and cooled atoms. Raman transitions induced by co-propagating Raman beams are insensitive to the atomic velocity and can be used in Doppler-free spectroscopy and in precision measurements. One example is a cold atom gyroscope which uses stimulated Raman transitions to manipulate the atomic wave packets [1]. Raman transitions driven with counter-propagating beams have a high velocity sensitivity and are successfully used in laser cooling of atoms. For instance, Raman sideband cooling techniques providing sub-recoil temperatures of trapped atoms have already shown their efficiency and reliability [2, 3]. These experiments require the jitter of the relative phase between the Raman laser beams to be negligible during the entire interaction time. Thus, the generation of two phase-coherent laser beams with a precise and tunable frequency difference at several GHz is an important prerequisite for their realization.

✉ Fax: +49-228/733-474, E-mail: dotsenko@iap.uni-bonn.de

We describe an apparatus that generates the required light fields to coherently couple the two cesium $6S_{1/2}$ hyperfine ground states. For this purpose we use a single laser source and an electro-optic modulator (EOM) to phase-modulate the laser at 9.2 GHz. An interferometer separates the sidebands from the carrier to permit a counter-propagating beam configuration. Acousto-optic modulators (AOMs) in each of the two laser beams provide additional intensity and frequency control.

A theoretical investigation of the interaction of the resulting three-frequency laser field with a three-level atom indicates the existence of two possible Raman transitions that interfere destructively. We experimentally observe the predicted effect and demonstrate that it can be avoided by shifting the carrier with respect to the sideband frequencies. As an application of our apparatus, we perform Raman spectroscopy of the ground state Zeeman sublevels of cesium atoms trapped in a standing wave dipole trap. In particular, we record spectra of motional sidebands as a prerequisite for Raman cooling.

2 Generation of the Raman beams

To drive a two-photon transition between the cesium hyperfine ground states $F = 3$ and $F = 4$, one needs two phase-coherent laser beams (pump and Stokes) with a frequency difference of the hyperfine splitting ($\omega_{\mathrm{hfs}}/2\pi = 9.2$ GHz). To perform Raman spectroscopy the frequency difference has to be tunable. Furthermore, for Raman sideband cooling, pump and Stokes beams have to be shined in from different directions to couple different motional states.

A widely used method to generate Raman beams with a frequency separation of 9.2 GHz is to phase lock two lasers at this frequency difference [4]. An alternative approach is the use of modulation techniques for generating sidebands at the modulation frequency. This can be achieved e.g. by direct current modulation of a diode laser at 4.6 GHz [5] or 9.2 GHz [6, 7]. Alternatively, one can amplitude- or phase-modulate a laser beam by an AOM (4.6 GHz [8]) or EOM (4.6 GHz or 9.2 GHz [9]), respectively. Because of the low modulation/deflection efficiency of high-frequency AOMs and EOMs, an amplification of the laser beam power by injection of two slave lasers is applied in the above-mentioned experiments.

In our experiment we use an EOM to produce optical sidebands at ±9.2 GHz from the carrier frequency of a laser beam radiated by a single diode laser. However, in our case, no further amplification is necessary and the generated beams are directly used for spectroscopy. Absence of phase locks provides a robust and stable system with highly precise frequency control.

Our setup is presented in Fig. 1. The laser is a single-mode diode laser ($\lambda = 852$ nm) in Littrow-configuration. Its output power is 30 mW. The laser is freely running and its detuning of $\Delta/2\pi = 10$–300 GHz from the Cs D_2-transition is monitored by a wavemeter (Coherent, W0121) with an accuracy of 0.1 GHz. The frequency drift is less than 0.5 GHz per hour, and hence the detuning is stable at the percent level. The EOM (New Focus, 4851 0.5–0.9 μm 9.2 GHz) is driven by a synthesizer (Agilent, 83751A .01–20 GHz) through a power amplifier (Industrial Electronics, AM53-9-9.4-33-35) with an rf power of +36 dBm. The synthesizer is locked to an external 10 MHz rubidium frequency standard (Stanford Research Systems, PRS10) to provide an absolute accuracy of 0.1 Hz at 9.2 GHz. The tuning range of the EOM is 50 MHz.

Drifts of the EOM temperature result in a slight deflection of the Raman beams and, hence, change their alignment with respect to the subsequent elements. Moreover, heating due to dissipation of microwave power produces drifts of the resonance frequency. To avoid these thermal effects, the EOM temperature is kept at 17 °C.

The relative power in the carrier and the first-order sidebands are monitored by a scanning cavity with a free spectral range of 1.5 GHz and amount to about 54% and 2 × 21%, respectively (see Fig. 2).

The sidebands are separated from the carrier with a Mach–Zehnder interferometer ([11], see Fig. 3). The difference of the two optical paths of the interferometer is set to provide opposite interference conditions for the optical frequencies of the sidebands, ω_{-1} and ω_1, and the carrier, ω_0, at the second beamsplitter and, hence, to spatially separate them. The interferometer is actively stabilized by locking the prism position such that maximum power comes out from the "carrier" output of the interferometer. This is possible because the power of the carrier beam is higher than the total power of the sidebands. For this lock the path length difference is scanned with a piezo actuator (PZT) by changing the position of the retro-reflecting prism. To observe the quality of the beam separation, we use a monitor interferometer. We achieve an interference contrast of about 80%, i.e. 10% of the light intensity goes into the wrong output. This number is limited by the imperfections of the optical components of the interferometer, e.g. the absence of anti-reflection coating and an asymmetric splitting ratio of the beamsplitter cubes.

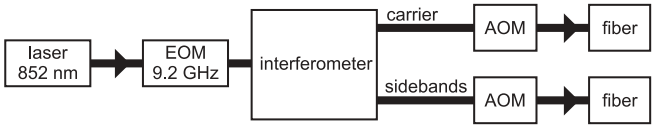

FIGURE 1 Scheme for generating the Raman beams. The laser beam from a single-mode laser diode is phase-modulated by an EOM at 9.2 GHz. The sidebands are then interferometrically separated from the carrier. Two AOMs serve for additional frequency and intensity control of both beams. The fibers act as spatial filters and transfer the beams to the experiment

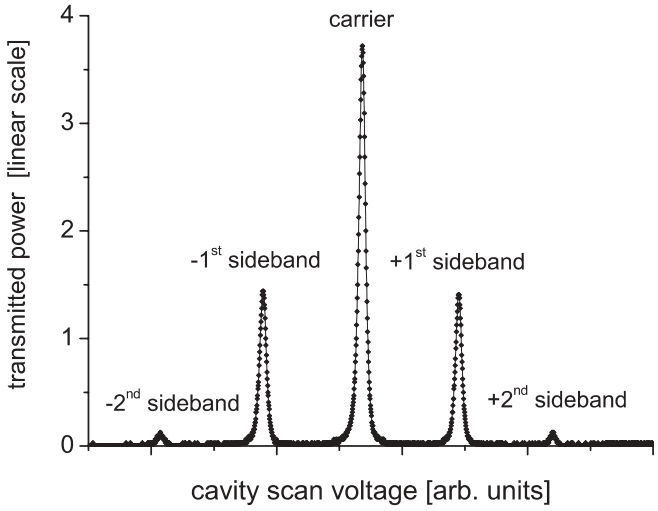

FIGURE 2 Measurement of the relative intensities of the carrier and the sidebands. The signal is obtained by analyzing the spectrum of the phase-modulates beam by means of a scanning Fabry–Perot interferometer. Note, that transmission maxima of the sidebands correspond to different orders of the interferometer which has a FSR of 1.5 GHz

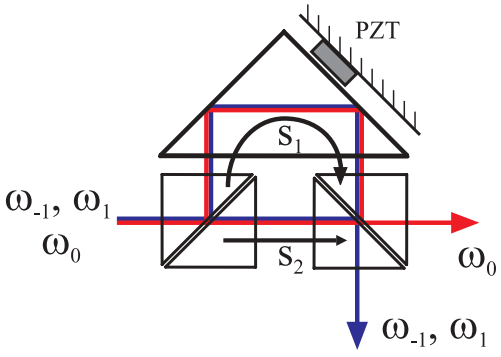

FIGURE 3 Separation of Raman beams using a Mach–Zehnder interferometer [11]. The optical path length difference, $s_1 - s_2$, is set such that the carrier, ω_0, and the sidebands, ω_1 and ω_{-1}, follow different outputs of the interferometer

To provide additional frequency and intensity control of the separated Raman beams, we installed acousto-optic modulators in each of the beams. They are set up in double-pass configuration and shift the respective optical frequencies by 200–240 MHz depending on the experimental needs. Both AOM drivers are externally locked to a 10 MHz frequency standard.

The Raman beams are sent to the experiment through two single-mode polarization-maintaining optical fibers which at the same time provide spatial filtering of the Raman beams. The described setup yields powers of the carrier and sideband beams on the order of 200 μW and 100 μW, respectively. To achieve high laser intensities at the position of the atoms, we focus the Raman beams down to a waist of 70 μm.

3 Interference of two Raman transitions

To expose the peculiarities of the introduced setup, which arise from the simultaneous presence of both sidebands in the experiment, we consider a simple theoretical model of the interaction between the Raman laser field and the atom.

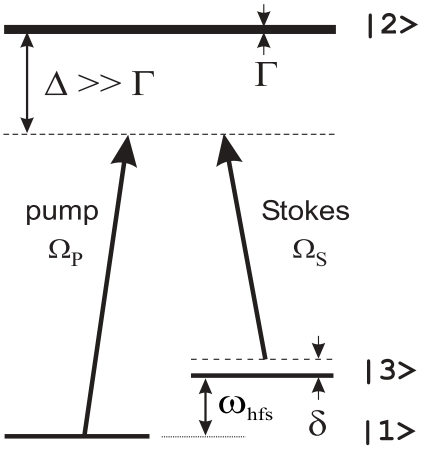

FIGURE 4 Three-level atom with two Raman lasers (pump and Stokes)

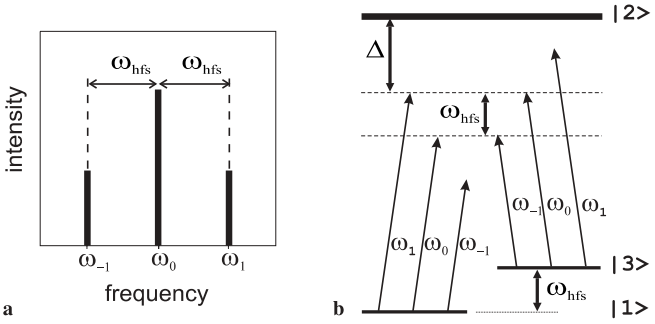

FIGURE 5 Coupling of three Raman lasers to a three-level atom. **a** Spectrum of the Raman beams generated by phase-modulation of a single laser beam **b** Level scheme showing two possible Raman transitions

A Raman transition is a stimulated scattering of a photon from one laser field into the other. This is realized by coupling two laser fields to a three-level atom in Λ-configuration (see Fig. 4) where levels $|1\rangle$ and $|3\rangle$ are coherently coupled by the Raman lasers (pump and Stokes) via the intermediate level $|2\rangle$. If the laser frequencies are ω_{P} and ω_{S}, respectively, and the separation of the two lower levels is ω_{HFS}, then the two-photon detuning is defined as $\delta = \omega_{\mathrm{P}} - \omega_{\mathrm{S}} - \omega_{\mathrm{HFS}}$. The coupling strength of a laser field with amplitude $\boldsymbol{E}_k$ to the atomic transition $|n\rangle = |1\rangle, |3\rangle \rightarrow |2\rangle$ is characterized by the Rabi frequency, defined as $\Omega_{k,\,n} = \langle n| - \hat{\boldsymbol{d}} \cdot \boldsymbol{E}_k/\hbar \; |2\rangle$. Here, $\hat{\boldsymbol{d}}$ is the dipole operator. To avoid resonant excitation to and spontaneous emission from the excited state, the detuning Δ from the one-photon resonance has to be much larger than the width Γ of the excited level and the Rabi frequencies Ω_{P} and Ω_{S}.

The Hamiltonian, which describes the coupling of the three levels by two coherent radiation fields within the rotating wave approximation, reads [12]

$$\hat{H} = \frac{\hbar}{2} \begin{pmatrix} 0 & \Omega_{\mathrm{P}} & 0 \\ \Omega_{\mathrm{P}} & 2\Delta & \Omega_{\mathrm{S}} \\ 0 & \Omega_{\mathrm{S}} & 2\delta \end{pmatrix}. \tag{1}$$

The solution of the corresponding Schrödinger equation yields the time evolution of the system, showing an oscillation of the populations of $|1\rangle$ and $|3\rangle$ at the generalized Rabi frequency $\tilde{\Omega}_{\mathrm{R}} = (\Omega_{\mathrm{R}}^2 + \tilde{\delta}^2)^{1/2}$, where $\tilde{\delta} = \delta + \Omega_{\mathrm{P}}^2/(4\Delta) - \Omega_{\mathrm{S}}^2/(4\Delta)$ is the generalized two-photon detuning which includes light shifts of levels $|1\rangle$ and $|3\rangle$, and

$$\Omega_{\mathrm{R}} = \frac{\Omega_{\mathrm{P}}\Omega_{\mathrm{S}}}{2\Delta} \tag{2}$$

is the resonant two-photon Rabi frequency.

Now, in our setup we deal with three different laser frequencies: the carrier ω_0 and the two sidebands ω_{-1} and ω_1 (see Fig. 5a). When coupled to a three-level atom the beams produce two possible Raman transitions as shown in Fig. 5b: one transition involves ω_1 and ω_0 and the other ω_0 and ω_{-1} as pump and Stokes beams, respectively.

The semi-classical treatment of the system is briefly presented below. We follow the derivation in [12] and extend it to the case of three beams interacting with a three-level atom. The full Hamiltonian $\hat{H}(t) = \hat{H}^0 + \hat{V}(t)$ includes the unperturbed part $\hat{H}^0$ and the operator $\hat{V}(t) = -\hat{\boldsymbol{d}} \cdot \boldsymbol{E}(t)$ of the time-dependent electric dipole interaction. The electric field consists of three monochromatic waves $\boldsymbol{E}(t) = \sum_{k=-1}^{1} \boldsymbol{E}_k \cos(\omega_k t - \varphi_k)$, where the φ_k denote the wave phases. The separation of neighboring frequencies is $\omega_{\mathrm{hfs}} + \delta$, where δ is introduced to account for the differential light shift of the ground levels caused by the Raman beams. For simplicity, the dipole moments of both one-photon transitions are considered to be equal. Introducing the Rabi frequency of the electric dipole interaction as $\Omega_{k,\,n} = \langle n| - \hat{\boldsymbol{d}} \cdot \boldsymbol{E}_k/\hbar \; |2\rangle$ $(n = 1,\ 3)$, we get $V(t) = V_1(t) + V_3(t)$, where

$$V_n(t) = \sum_{k=-1}^{1} \hbar\Omega_{k,\,n} \cos(\omega_k t - \varphi_k). \tag{3}$$

The state vector $\boldsymbol{\Psi}(t)$ can be expressed as a superposition of the eigenstates $|n\rangle$ of $\hat{H}^0$:

$$\boldsymbol{\Psi}(t) = \sum_{n=1}^{3} C_n(t)\, \mathrm{e}^{-\mathrm{i}\xi_n(t)} |n\rangle, \tag{4}$$

where $\xi_n(t)$ are time-dependent state phases. The coefficients $C_n(t)$ are the probability amplitudes which, squared, yield the population of state $|n\rangle$. Thus, the time-dependent Schrödinger equation can be derived in the differential form

$$\mathrm{i}\hbar \frac{\mathrm{d}}{\mathrm{d}t} C_m(t) = \left[E_m^0 - \hbar\dot{\xi}_m(t)\right] \cdot C_m(t) + \sum_{n=1}^{3} V(t)\, C_n(t)\, \mathrm{e}^{\mathrm{i}[\xi_m(t) - \xi_n(t)]}. \tag{5}$$

Next, we define the state phases as $\dot{\xi}_n = E_n^0/\hbar$ for $n = 1, 2$ and $\dot{\xi}_3 = E_3^0/\hbar + \delta$. Since $\Delta \gg (\omega_{\mathrm{hfs}},\ \Omega_i)$, we expect the population of the excited state to be small compared to the other states and to vary quickly. Thus, we adiabatically eliminate this state and reduce our three-level system to an effective two-level system. To eliminate the high-frequency components, i.e. exponentials oscillating at the sum of optical frequencies, we apply the rotating-wave approximation. Denoting $\bar{\varphi}_1 = \varphi_0 - \varphi_1$ and $\bar{\varphi}_{-1} = \varphi_{-1} - \varphi_0$ we obtain the effective two-level interaction matrix, which couples the levels $|1\rangle$

and $|3\rangle$,

$$\hat{W} = \frac{1}{4}\begin{pmatrix} \frac{\Omega_1^2}{\Delta} + \frac{\Omega_0^2}{\Delta+\omega_{\rm hfs}} + \frac{\Omega_{-1}^2}{\Delta+2\omega_{\rm hfs}} & \cdots \\ \frac{\Omega_1\Omega_0}{\Delta}\mathrm{e}^{-\mathrm{i}\bar{\varphi}_1} + \frac{\Omega_0\Omega_{-1}}{\Delta+\omega_{\rm hfs}}\mathrm{e}^{-\mathrm{i}\bar{\varphi}_{-1}} & \\ & \cdots \\ \cdots & \frac{\Omega_1\Omega_0}{\Delta}\mathrm{e}^{\mathrm{i}\bar{\varphi}_1} + \frac{\Omega_0\Omega_{-1}}{\Delta+\omega_{\rm hfs}}\mathrm{e}^{\mathrm{i}\bar{\varphi}_{-1}} \\ \cdots & \frac{\Omega_1^2}{\Delta-\omega_{\rm hfs}} + \frac{\Omega_0^2}{\Delta} + \frac{\Omega_{-1}^2}{\Delta+\omega_{\rm hfs}} + 4\delta \end{pmatrix}. \tag{6}$$

The difference of the diagonal elements is due to the differential light shift caused by the Raman lasers acting on each level. This shift has to be compensated for in the experiment to meet the two-photon resonance condition.

The two-photon Rabi frequency at resonance is calculated from the off-diagonal elements of (6) and reads

$$\Omega_{\rm R} = \sqrt{\Omega_{\rm R1}^2 + \Omega_{\rm R2}^2 + 2\Omega_{\rm R1}\Omega_{\rm R2}\cos\overline{\varphi}}\,, \tag{7}$$

where

$$\Omega_{\rm R1} = \frac{\Omega_1\Omega_0}{2\Delta} \quad \text{and} \quad \Omega_{\rm R2} = \frac{\Omega_0\Omega_{-1}}{2(\Delta+\omega_{\rm hfs})}, \tag{8}$$

and $\overline{\varphi} = \varphi_1 + \varphi_{-1} - 2\varphi_0$. Equation (7) shows that the two Raman transitions with Rabi frequencies $\Omega_{\rm R1}$ and $\Omega_{\rm R2}$ interfere, depending on the phase $\overline{\varphi}$.

The phase modulation produces sidebands with opposite phases ($\overline{\varphi} = \pi$) and, thus, the two Raman transitions interfere destructively yielding a two-photon Rabi frequency $\Omega_{\rm R}^{\rm destr}$ reduced by a factor $\eta = \omega_{\rm hfs}/(\Delta+\omega_{\rm hfs})$:

$$\Omega_{\rm R}^{\rm destr} = \eta\,\frac{\Omega_1\Omega_0}{2\Delta}\,. \tag{9}$$

Here, we have set $\Omega_1 = \Omega_{-1}$ since the powers of the two sidebands are equal. For small detunings ($\Delta \ll \omega_{\rm hfs}$, and thus $\eta = 1$) the contribution of the transition involving ω_1 and ω_0 is much larger than of the other transition and $\Omega_{\rm R}^{\rm destr}$ approaches $\Omega_{\rm R}$ of (2). For large detunings ($\Delta \gg \omega_{\rm hfs}$) η scales as Δ^{-1} and, thus, significantly reduces the Rabi frequency.

Moreover, if the Raman beams are spatially separated and propagate along different optical paths, they get an arbitrary phase difference $\overline{\varphi}$ which is sensitive to fluctuations of the path length of the order of the optical wavelength, leading to large fluctuations in $\Omega_{\rm R}$.

To avoid any of these interference effects, we can suppress one of the Raman transitions by shifting the frequency of one sideband, e.g. of ω_{-1}, by $2\delta_{\rm AOM}$ and obtain (see Fig. 6a)

$$\begin{cases} \omega_1 - \omega_0 = \omega_{\rm hfs} \\ \omega_0 - \omega_{-1} = \omega_{\rm hfs} - 2\delta_{\rm AOM}\,. \end{cases} \tag{10}$$

As a result, the second transition is shifted by $2\delta_{\rm AOM}$ out of the two-photon resonance, as shown in Fig. 6b. For $2\delta_{\rm AOM} \gg \Omega_{\rm R2}$ this transition can be neglected and the two-photon Rabi frequency reduces to $\Omega_{\rm R}$, given by (2).

Since we cannot change the frequencies of the sidebands individually, it is straight-forward to shift the carrier frequency by $-\delta_{\rm AOM}$ to produce the desired asymmetry in the Raman beams spectrum. This is done by driving the AOMs

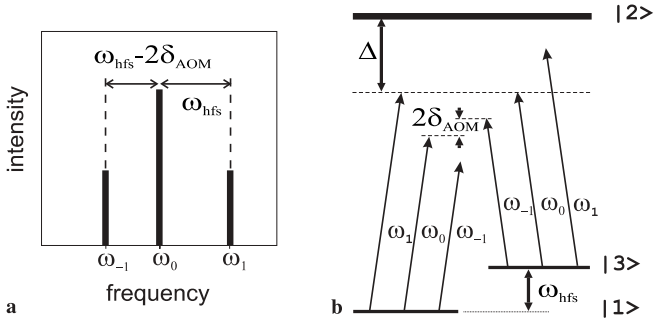

FIGURE 6 Suppression of one of the two Raman transitions **a** The frequency of the lower sideband ω_{-1} is shifted by $2\delta_{\rm AOM}$ **b** Coupling scheme with only one possible Raman transition remaining

placed in each of the Raman beams at the frequency difference $\omega_{\rm AOM}^{\rm sideband} - \omega_{\rm AOM}^{\rm carrier} = \delta_{\rm AOM}/2$, where the factor of 2 is due to a double-pass configuration of the AOMs. Then, to match the frequency spacing between the carrier and the first positive sideband with the hyperfine splitting $\omega_{\rm hfs}$, we set the EOM modulation frequency to $\omega_{\rm hfs} - \delta_{\rm AOM}$. Typically, we have $\delta_{\rm AOM}/2\pi = 20$ MHz.

4 Experiment

To demonstrate the application of our setup, we performed Raman spectroscopy of the ground state Zeeman sublevels and of vibrational sidebands with a small number of trapped cesium atoms.

4.1 *Atomic traps*

The experimental setup is described in detail elsewhere [13, 14]. In brief, a high-field magneto-optical trap (MOT) traps cesium atoms from the background gas in a vacuum cell. The fluorescence photons from the atoms are collected by a diffraction-limited objective [15] and detected by an avalanche photodiode. To count the number of atoms in the MOT, we compare their fluorescence rate to the single atom fluorescence rate. This allows us to unambiguously determine up to 20 atoms.

The atoms are then transferred into a dipole trap. Our standing-wave dipole trap consists of two counter-propagating fundamental Gaussian laser beams of equal intensities, frequencies and parallel linear polarizations generated by a Nd : YAG laser ($\lambda = 1064$ nm). The resulting interference pattern produces a position-dependent light shift of the Cs ground state, which forms a periodic trapping potential with a period of half a wavelength. We are able to transfer atoms between the MOT and the dipole trap without loss when we superimpose both traps for several 10 ms.

To compensate dc magnetic fields as well as to apply a guiding magnetic field for defining a quantization axis, three pairs of orthogonal magnetic coils are placed around the MOT. By controlling the three coil currents, we can create a magnetic field of arbitrary direction and amplitude of up to 1 G.

4.2 *Experimental sequence*

To record Raman spectra or to observe Rabi oscillations, we have to measure the transition probability be-

tween the hyperfine states depending on the Raman detuning or Raman pulse duration, respectively. For this purpose, we have to prepare the initial and to detect the final hyperfine state of the atom. We prepare the atoms in the $F = 4$ state using optical pumping by the MOT repumping laser which is resonant to the $F = 3 \rightarrow F' = 4$ transition [17]. To be insensitive to fluctuations of the magnetic field, we work on the $|F = 4,\ m_F = 0\rangle \rightarrow |F = 3,\ m_F = 0\rangle$ transition. While a guiding magnetic field of about 1 G is applied, a π-polarized laser resonant with the transition $F = 4 \rightarrow F' = 4$ optically pumps atoms into the dark $m_F = 0$ state. At the same time a π-polarized laser resonant with $F = 3 \rightarrow F' = 4$ serves as a repumping laser. This way about 60% of the atoms are prepared in the $|F = 4,\ m_F = 0\rangle$ state. The Raman lasers are both σ^+ polarized and together drive a $\Delta m_F = 0$ transition (see Fig. 7).

For state detection we use an intense "push-out" laser resonant with the nearly-closed transition $F = 4 \rightarrow F' = 5$, which pushes the atoms out of the dipole trap if they are in the $F = 4$ level [17]. The atoms in the $F = 3$ level, however, are unaffected and remain trapped. To reduce the number of photons necessary for the pushing-out and to prevent accidental pumping to $F = 3$, we lower the dipole trap depth adiabatically to about 5% of the maximum depth prior to the push-out.

After the state-selective push-out is performed, the remaining atoms are transferred back into the MOT and their fluorescence rate R_{final} is measured. When the MOT magnetic field is switched off, the atoms leave the trap, and we measure the stray light level R_{backgr} of the MOT lasers. Using the initial fluorescence rate R_{initial} we determine the ratio of atoms transferred from the $F = 4$ state to $F = 3$ by the Raman field. The population transfer is then given by

$$P = \frac{R_{\text{final}} - R_{\text{backgr}}}{R_{\text{initial}} - R_{\text{backgr}}}. \tag{11}$$

The typical time dependence of the fluorescence signal for a Raman spectroscopy experiment is shown in Fig. 8. The described techniques of the state preparation and detection have been proven to be efficient at the single atom level. However, to get better statistics, we repeated the measurement many times with about 40–60 atoms at a time.

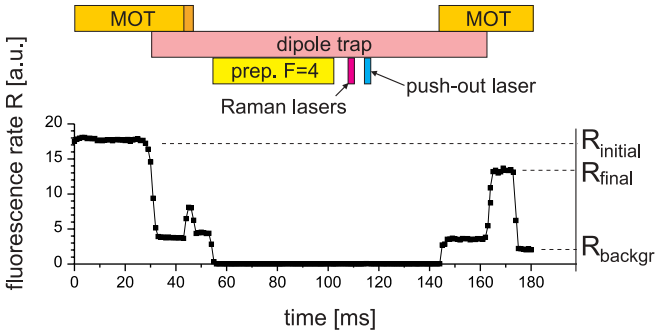

FIGURE 8 Experimental sequence for a Raman spectroscopy experiment averaged over 10 repetitions. The information obtained is the initial, final and background fluorescence rates

4.3 *Spectroscopy of Zeeman sublevels*

Due to their magnetic field dependence, Raman transitions between Zeeman sublevels can be used to measure the magnetic field amplitude in a specific direction and thereby to monitor the quality of the magnetic field compensation. Another important application of this spectroscopy is the measurement of the resonance frequency $|F = 4,\ m_F = 0\rangle \rightarrow |F = 3,\ m_F = 0\rangle$ which is modified by the differential light shift of the ground hyperfine states produced by the off-resonant lasers shined onto the atoms, namely Raman and Nd : YAG lasers. For this purpose, we measure the position of the central line in the Raman spectrum of the Zeeman sublevels.

A typical spectrum without the optical pumping into $m_F = 0$ is presented in Fig. 9. Each point results from 20 measurements with approximately 15 atoms per measurement. In order not to excite the vibrational sidebands, the Raman beams are co-propagating. The guiding magnetic field is parallel to the σ^+-polarized Raman beams. Here, the pow-

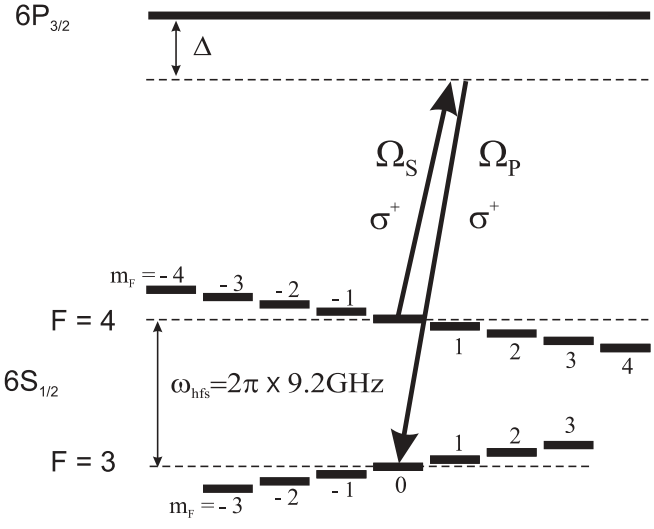

FIGURE 7 Zeeman splitting of the Cs ground states in the presence of a magnetic field. The two σ^+-polarized Raman lasers induce $\Delta m_F = 0$ transitions

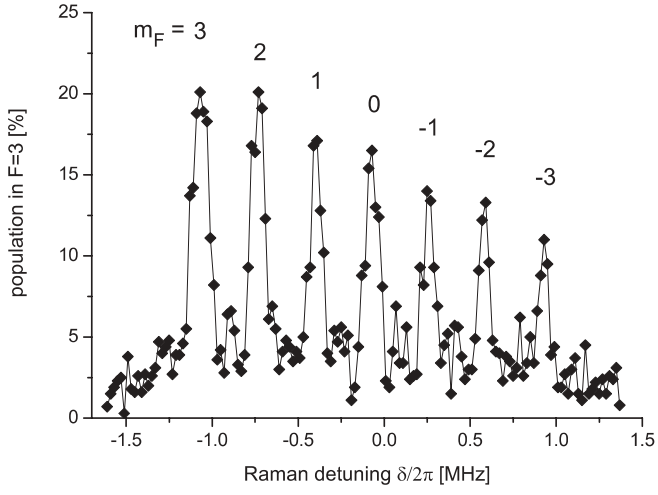

FIGURE 9 The Raman spectrum of the Zeeman sublevels. Seven peaks correspond to seven possible transitions with $\Delta m_F = 0$

ers of the Raman sideband and carrier beams are $P_P = 80\,\mu W$ and $P_S = 166\,\mu W$, respectively, the duration of the Raman pulses is $\tau = 10\,\mu s$ and the detuning is $\Delta/2\pi = 13.7\,GHz$. The dipole trap depth is 1.3 mK. The peaks have a FWHM of about 100 kHz and are thus Fourier-limited. The asymmetry of the peak heights is most probably due to residual optical pumping.

4.4 *Spectroscopy of vibrational sidebands*

An atom tightly bound in a trapping potential shows vibrational sidebands in the absorption spectrum, separated from the atomic resonance frequency by the oscillation frequency. To resolve the vibrational sidebands, a transition with a linewidth small compared to the oscillation frequency is required. Furthermore, to couple different motional states enough momentum transfer has to be provided. To satisfy these requirements, Raman transitions induced by non-copropagating laser beams can be used.

We record a Raman spectrum of the axial vibrational sidebands (see Fig. 10) by shining in counter-propagating Raman beams parallel to the dipole trap lasers. The frequencies of the AOMs and the EOM are chosen such as to suppress one of the two Raman transitions as described in Sect. 3. The parameters of the Raman beams are $P_P = 120\,\mu W$, $P_S = 360\,\mu W$, $\Delta/2\pi = 150\,GHz$, and $\tau = 2\,ms$. For each point in the spectrum, we have summed up the results of 10 measurements with an ensemble of about 40–60 atoms each. The central peak corresponds to transitions between the same vibrational levels; peaks to the left and to the right are transitions to lower and higher vibrational levels, respectively. The positions of the peak maxima are equidistant with a frequency separation of 70 kHz, which is the oscillation frequency $\Omega_z/2\pi$ in axial direction of the dipole trap. This value is in agreement with the oscillation frequency of 71 ± 3 kHz calculated in harmonic approximation from the respective trap depth of $45 \pm 4\,\mu K$ [16]. The asymmetry of the peaks, which correspond to the transitions between different vibrational levels, is due to the anharmonicity of the trapping potential seen by atoms with a high energy.

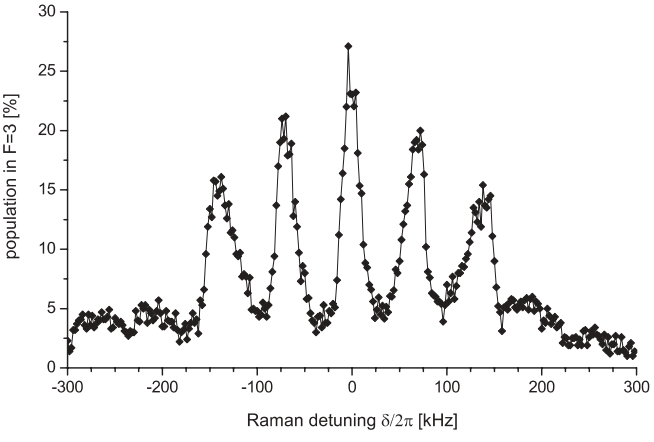

FIGURE 10 Raman spectrum of the vibrational sidebands. Central peak corresponds to transitions between the same vibrational levels. Peaks to the left and to the right are transitions to lower and higher vibrational levels, respectively

4.5 *Rabi oscillations and the interference effect*

Rabi oscillations are recorded with co-propagating Raman beams resonant to the $|F = 4,\ m_F = 0\rangle \rightarrow |F = 3,\ m_F = 0\rangle$ transition the frequency of which is measured from the Zeeman spectrum. The measured Rabi oscillations, i.e. the dependence of the population transfer into the $F = 3$ level on the duration of the Raman pulse, is shown in Fig. 11a. Here, the dipole trap depth is 0.1 mK. The powers and detuning of the Raman beams are the same as used in Sect. 4.4.

The measured two-photon Rabi frequency is $\Omega_R/2\pi = 13.4$ kHz, while a theoretical calculation predicts a value of 38 kHz. The discrepancy can be explained by the imperfect separation of the carrier and sidebands by the interferometer. In combination with the AOMs (see Fig. 1), this results in minor additional frequency components which induce two resonant Raman transitions that interfere destructively with the main Raman transition induced by the carrier and the higher sideband. Despite the low intensities of the parasitic frequency components (only 10% of the total power), they are still expected to reduce the Rabi frequency by a factor of $\eta_{separation} = 3.0 \pm 0.3$. This is in good agreement with our observation.

To observe the interference of the two possible Raman transitions shown in Fig. 5, we record Rabi oscillations with

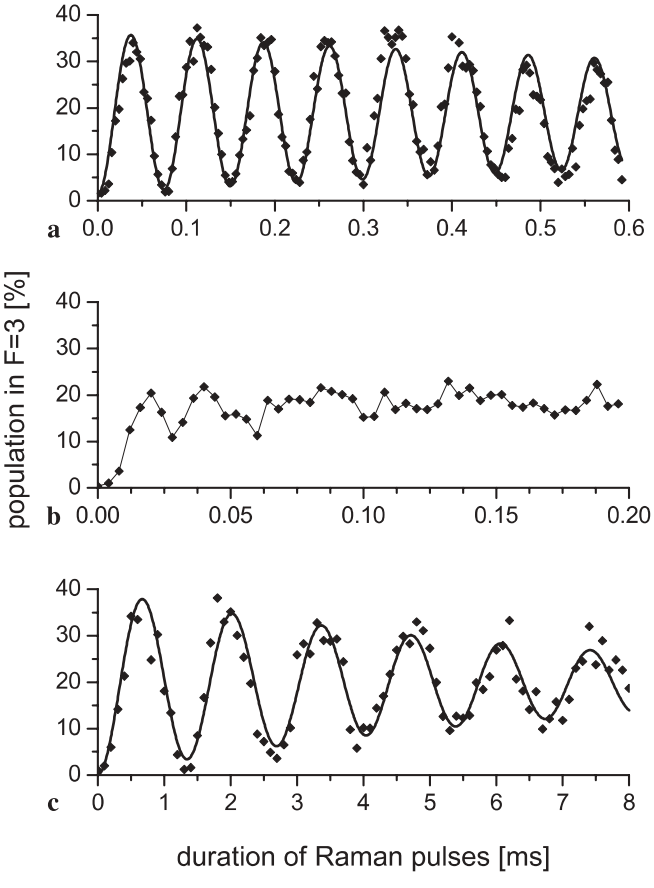

FIGURE 11 Rabi oscillations induced by the Raman field. The fitting functions are the exponentially decaying sinusoidal oscillations **a** No interference since only one Raman transition is resonant **b** Interference with the fluctuating relative phase **c** Destructive interference. Note, that the laser beam intensities in **a** and **b** are the same and differ from those in **c**

both transitions being resonant. For this purpose, we set the frequencies of the AOMs to the same value, while the EOM frequency is set to match the hyperfine splitting ω_{hfs}. The Raman beams are separated with the interferometer and overlapped on the experiment table to be co-propagating. The recorded oscillations are shown in Fig. 11b. The fast decay of the oscillations can be explained by jitters of optical elements which, being of the order of the optical wavelength, randomly change the phase of the light field. Consequently, the phase difference $\overline{\varphi}$ of the separated Raman beams fluctuates resulting in a random instantaneous two-photon Rabi frequency.

The presence of pure destructive interference can be observed if the Raman beams are not separated. For this purpose, we disable the interferometer by blocking its retro-reflecting prism and use only one of its outputs. The measured oscillations with the reduced Rabi frequency (740 Hz) are shown in Fig. 11c. Note that the powers of the Raman beams differ from those in the previous experiment and are $P_{\mathrm{P}} = 25\,\mu\mathrm{W}$ and $P_{\mathrm{S}} = 53\,\mu\mathrm{W}$, respectively. Taking into account these beam powers and the interference effect (9), we expected that the reduced Rabi frequency $\Omega_{\mathrm{R}}^{\mathrm{destr}}$ would be 420 Hz. The higher experimental value of 740 Hz is due to the presence of the second-order sidebands. Each of them possesses about 1.8% of the total optical power and, together with the first-order sidebands, can also drive Raman transitions. Since the corresponding Rabi frequencies are small, they only play a role when the main Raman transitions interfere destructively and their effect was not noticeable in our previous experiments. Taking into account the phases of the sidebands, we expected that the theoretically calculated Rabi frequency to be increased by a factor of $\eta_{2\,\mathrm{sb}} = 1.55 \pm 0.04$, which, thus, agrees well with the experimental findings.

5 Summary and outlook

In this paper, we have presented an experimental setup for generating Raman laser beams with a controllable frequency difference for experiments on Raman spectroscopy and Raman cooling of cesium atoms. The generation is based on the phase-modulation of a laser beam with an EOM at 9.2 GHz. The setup does not have phase-locking elements. However, a thorough alignment of the interferometer, which separates the Raman beams, is necessary. An interference effect between two Raman transitions, which arises from the peculiarities of the phase-modulation and reduces the two-photon Rabi frequency, has been fully understood and eliminated by a slight modification of the Raman beam spectrum.

Using the presented setup we have recorded Raman spectra of Zeeman levels and vibrational sidebands as well as Rabi oscillations between the hyperfine levels of trapped Cs atoms. All experiments are performed with a small number of atoms (40–60) and can be extended to the single atom level.

The resolved vibrational sidebands and the Rabi oscillations induced by the Raman laser field open the possibility for Raman sideband cooling [2, 3] of trapped individual atoms. This will enable us to transfer atoms into their lowest vibrational level providing ultimate control of their position.

ACKNOWLEDGEMENTS We have received support from the Deutsche Forschungsgemeinschaft and the state of North Rhine-Westfalia, and from the European Commission (QGates network).

REFERENCES

1 T.L. Gustavson, A. Landragin, M. Kasevich: Class. Quantum. Grav. **17**, 1 (2000)
2 R. Taïeb, R. Dum, J.I. Cirac, P. Marte, P. Zoller: Phys. Rev. A**49**, 4876 (1994)
3 C. Monroe, D.M. Meekhof, B.E. King, S.R. Jefferts, W.M. Itano, D.J. Wineland, P. Gould: Phys. Rev. Lett. **75**, 4011 (1995)
4 G. Santarelli, A. Clairon, S.N. Lea, G.M. Tino: Opt. Commun. **104**, 339 (1994)
5 J. Ringot, Y. Lecoq, J.C. Garreau, P. Szriftgiser: Eur. Phys. J. D **65**, 285 (1999)
6 K.Y. Lau, C. Harder, A. Yariv: Appl. Phys. Lett **44**, 273 (1984)
7 C. Affolderbach, A. Nagel, S. Knappe, C. Jung, D. Wiedenmann, R. Wynands: Appl. Phys. B **70**, 407 (2000)
8 P. Bouyer, T.L. Gustavson, K.G. Haritos, M.A. Kasevich: Opt. Lett. **21**, 1502 (1996)
9 K. Szymaniec, S. Ghezali, L. Cognet, A. Clairon: Opt. Comm. **144**, 50 (1997)
10 J.R. Kuklinski, U. Gaubatz, F.T. Hioe, K. Bergmann: Phys. Rev. A **40**, 6741 (1989)
11 D. Haubrich, M. Dornseifer, R. Wynands: Rev. Sci. Inst. **71**, 225 (2000)
12 B.W. Shore: *The Theory of Coherent Atomic Excitation* (Wiley, New York 1990)
13 S. Kuhr, W. Alt, D. Schrader, M. Müller, V. Gomer, D. Meschede: Science **293**, 278 (2001)
14 D. Schrader, S. Kuhr, W. Alt, M. Müller, V. Gomer, D. Meschede: Appl. Phys. B **73**, 819 (2001)
15 W. Alt: Optik **113**, 142 (2002)
16 W. Alt, D. Schrader, S. Kuhr, M. Müller, V. Gomer, D. Meschede: Phys. Rev. A **67**, 033 403 (2003)
17 S. Kuhr, W. Alt, D. Schrader, I. Dotsenko, Y. Miroshnychenko, W. Rosenfeld, M. Khudaverdyan, V. Gomer, A. Rauschenbeutel, D. Meschede: Phys. Rev. Lett. **91**, 213 002 (2003)